NASA/TM—2001-211219

A Three-Dimensional CFD Investigation of Secondary Flow in an Accelerating, 90° Elbow

Richard H. Cavicchi
Glenn Research Center, Cleveland, Ohio

December 2001

The NASA STI Program Office . . . in Profile

Since its founding, NASA has been dedicated to the advancement of aeronautics and space science. The NASA Scientific and Technical Information (STI) Program Office plays a key part in helping NASA maintain this important role.

The NASA STI Program Office is operated by Langley Research Center, the Lead Center for NASA's scientific and technical information. The NASA STI Program Office provides access to the NASA STI Database, the largest collection of aeronautical and space science STI in the world. The Program Office is also NASA's institutional mechanism for disseminating the results of its research and development activities. These results are published by NASA in the NASA STI Report Series, which includes the following report types:

- TECHNICAL PUBLICATION. Reports of completed research or a major significant phase of research that present the results of NASA programs and include extensive data or theoretical analysis. Includes compilations of significant scientific and technical data and information deemed to be of continuing reference value. NASA's counterpart of peer-reviewed formal professional papers but has less stringent limitations on manuscript length and extent of graphic presentations.

- TECHNICAL MEMORANDUM. Scientific and technical findings that are preliminary or of specialized interest, e.g., quick release reports, working papers, and bibliographies that contain minimal annotation. Does not contain extensive analysis.

- CONTRACTOR REPORT. Scientific and technical findings by NASA-sponsored contractors and grantees.

- CONFERENCE PUBLICATION. Collected papers from scientific and technical conferences, symposia, seminars, or other meetings sponsored or cosponsored by NASA.

- SPECIAL PUBLICATION. Scientific, technical, or historical information from NASA programs, projects, and missions, often concerned with subjects having substantial public interest.

- TECHNICAL TRANSLATION. English-language translations of foreign scientific and technical material pertinent to NASA's mission.

Specialized services that complement the STI Program Office's diverse offerings include creating custom thesauri, building customized data bases, organizing and publishing research results . . . even providing videos.

For more information about the NASA STI Program Office, see the following:

- Access the NASA STI Program Home Page at ***http://www.sti.nasa.gov***

- E-mail your question via the Internet to help@sti.nasa.gov

- Fax your question to the NASA Access Help Desk at 301–621–0134

- Telephone the NASA Access Help Desk at 301–621–0390

- Write to:
  NASA Access Help Desk
  NASA Center for AeroSpace Information
  7121 Standard Drive
  Hanover, MD 21076

NASA/TM—2001-211219

A Three-Dimensional CFD Investigation of Secondary Flow in an Accelerating, 90° Elbow

Richard H. Cavicchi
Glenn Research Center, Cleveland, Ohio

National Aeronautics and
Space Administration

Glenn Research Center

December 2001

Acknowledgments

The author gratefully acknowledges access to the wisdom of Dr. John W. Slater of NASA Glenn Research Center in consultation in the early stage of this project.

Available from

NASA Center for Aerospace Information
7121 Standard Drive
Hanover, MD 21076

National Technical Information Service
5285 Port Royal Road
Springfield, VA 22100

Available electronically at http://gltrs.grc.nasa.gov/GLTRS

A THREE-DIMENSIONAL CFD INVESTIGATION OF SECONDARY FLOW IN AN ACCELERATING, 90° ELBOW

Richard H. Cavicchi
National Aeronautics and Space Administration
Glenn Research Center
Cleveland, Ohio 44135

SUMMARY

NASA Glenn Research Center has recently applied the WIND National Code flow solver to an accelerating elbow with a 90° bend to reveal aspects of secondary flow. This elbow was designed by NACA in the early 1950's such that flow separation would be avoided. Experimental testing was also done at that time. The current three-dimensional CFD investigation shows that separation has indeed been avoided. Using its three-dimensional capability, this investigation provides various viewpoints in several planes that display the inception, development, and final location of a passage vortex. Its shape first becomes discernible as a vortex near the exit of the bend. This rendition of the exit passage vortex compares well with that found in the experiments. The viewpoints show that the passage vortex settles on the suction surface at the exit about one-third of the distance between the plane wall and midspan. Furthermore, it projects into the mainstream to about one-third of the channel width. Of several turbulence models used in this investigation, the Spalart Alimaras, Baldwin Lomax, and SST (Shear Stress Transport) models were by far the most successful in matching the experiments.

INTRODUCTION

A classic investigation of secondary flow, both theoretical and experimental, was made at the National Advisory Committee For Aeronautics (NACA) Lewis Flight Propulsion Laboratory in the early 1950's. This work, reported in references 1 and 2, used an accelerating, rectangular 90° elbow as the geometric configuration. The project began with the design of the elbow by the so-called "inverse method." In this mode of design, velocity distributions along the initially unspecified boundaries are prescribed, following which analysis is used to determine the boundary shapes. The more common "direct method" prescribes the shapes of the boundaries, and then uses analysis to determine the velocity distributions.

Reference 1 describes the analysis it used in the following way. In the inverse method, the geometry of the channel walls in the X-Y plane is unknown. This fact precludes obtaining a solution in the physical plane, necessitating the use of a new set of coordinates in a transformed plane. The geometric boundaries must be known in the transformed plane. The coordinates in the transformed plane should be orthogonal in the physical plane. Reference 1 used the velocity potential phi and stream function psi as coordinates in the transformed plane, and derived a differential equation for the velocity distribution in this plane. Solution of this equation for the velocity distribution yielded the distribution of the flow direction. Finally, the flow direction distribution yielded the distribution of the channel walls in the physical X-Y plane. The differential equation was obtained from continuity and from irrotational fluid motion expressed in terms of ϕ and ψ. This equation is nonlinear and was solved by relaxation. Hence, the shape of the elbow was obtained from two-dimensional inviscid flow analysis.

For the 90° elbow designed in reference 1, a velocity distribution was prescribed such that no deceleration occurred along the boundary walls in order to avoid boundary layer separation. This attempt to avoid separation was intended to provide high quality experimental data of the secondary flow mechanism itself.

Although the elbow was designed by two-dimensional analysis, the experimental configuration was made as a three-dimensional model with decreasing rectangular cross sections to yield exit velocity twice the inlet value.

The current effort is a three-dimensional computational fluid dynamic investigation using the WIND flow solver applied to the 90° elbow designed in reference 1. A complete description of WIND is presented in reference 3. This CFD study investigated the development of secondary flow from several viewpoints made available by three-dimensional analysis. These viewpoints are presented in selected planes to show the inception and buildup of

secondary flow that culminate in the formation of a passage vortex. In this way, the current CFD study not only documents a test case, but extends the insight of the secondary flow problem that the experiments of reference 2 have investigated.

Thus, this report provides a further validation of the WIND code. Validation using other configurations has been achieved, and is presented on the World Wide Web. The site in reference 4 presents several CFD cases in complete detail that are compared with experimental data.

Calculations were made herein for subsonic flow entering the elbow, and using the Spalart Allmaras one-equation turbulence model. For comparison, WIND was also run for this elbow using several other turbulence models in its capability. This investigation used the following post processing tools: CFPOST (described in ref. 3), PLOTC (described in ref. 5), and PLOT3D (described in ref. 6).

CONFIGURATION

Although the original design of the elbow used the indirect method, the current CFD application starts with the elbow shape and then computes the flow field. The profile shape of example III of reference 1 was chosen for use in the current CFD study.

Figure 1, taken from reference 2, presents a line drawing of the test setup and depicts the elbow shape. The XYZ coordinate system is shown in this figure. These coordinates are defined in appendix A. Because of symmetry about the midspan, only one-half of the elbow was modeled and run for this CFD investigation. The external profile side showing the 90° bend is referred to herein as the plane wall.

The entire set of X-Y coordinates for example III is presented as table II in reference 1. All 1170 of these coordinates were plotted and are shown in the current report in figure 2(a). Table II includes an 18-in. long constant cross section shape downstream extension that also appears in figure 2(a) herein.

In addition to prescribing the suction and pressure surface velocity distributions, reference 1 also sets the exit velocity to be twice the inlet value. The prescribed velocity Q as a function of arc length s along the channel walls is given by equation (35) of reference 1 as

$$Q = 0.5 \qquad s \le 0$$

$$Q = \frac{1}{2} + \frac{S^2}{6} - \frac{S^3}{27} \qquad 0 \le s \le 3.0$$

$$Q = 1.0 \qquad s \ge 3.0$$

Q and s are both nondimensional and are defined in Appendix A. The above specification was applied to both the inner and outer channel walls (suction and pressure surfaces), and is shown in figure 3(a), which is taken from reference 1.

GRIDS

Two three-dimensional structured grids were generated from the shape of figure 2(a) for use with WIND. A fine grid is provided for viscous turbulent flow and a coarse grid, for inviscid flow.

Grid Clustering

The grid consists of a single-zone, structured H-grid. The grid is clustered at the walls of the elbow. The first grid point off the wall is at a distance of 5.0×10^{-4} in., which was determined from a flow simulation of a flat plate boundary layer to provide a value of y+ of approximately 1.0. y+ is a nondimensional distance from the wall for which a value of 1.0 ensures proper resolution in the viscous sublayer. The grid was distributed along each grid line using the hyperbolic tangent distribution. The number of grid points was chosen to keep grid stretching between successive grid points below 15 percent.

Grid Indexing

The grids are represented by:

fine grid (for viscous runs):	75 by 61 by 35
coarse grid (for inviscid run):	75 by 41 by 9

for indices i, j, and k, respectively. These indices pertain to the following directions:

- i inlet to exit along flow direction
- j suction surface to pressure surface across channel
- k midspan to plane wall in spanwise direction

Both grids are single zone. A 24-in. inlet tunnel is included in the grids that were modeled.

Zone Boundaries

The following zone boundaries were applied to the CFD model:

i1	tunnel inflow plane
imax	elbow extension exit plane
j1	inner (suction) surface
jmax	outer (pressure) surface
k1	symmetry plane (midspan)
kmax	elbow plane wall

Grid Cross Sections

Figure 2(b) shows a profile of the 75 by 61 fine grid in the X-Y plane at the plane wall, and displays the range of indices i and j. Figure 2(c) shows the 61 by 35 cross section in the X-Z plane at the inlet. A three-dimensional view of the fine grid is presented in figure 2(d) to provide perspective, and to show planes of constant values of index i. Some of the grid lines in this figure have been omitted for clarity.

INPUT

The initial conditions specified for all the runs using WIND in this investigation are:

Mach Number	0.1
Total pressure	15.422 psia (20 in. water in ref. 2)
Total temperature	520 °R
Entrance angle from X-direction	90°

Preliminary Files

Appendix B presents three files that inform WIND of the exact details of the problem to be run. The INPUT DATA FILES include the initial conditions plus additional information needed for the run. The first of these two files provides the input data for an inviscid run. The second INPUT DATA FILE pertains to a viscous run. The third file in appendix B presents the command line form of the GMAN (grid management) file. This file incorporates

the three-dimensional boundary conditions into the grid file. At index k = 1 (the midplane), the boundary is set at "reflection" to denote symmetry. Hence, only one-half of the elbow was simulated in running WIND.

RESULTS AND DISCUSSION

Inviscid Results

Prescribed velocity distribution.—A first step in this investigation was to compare the surface velocity distributions obtained from inviscid WIND calculations with the prescribed distribution. Figure 3(a) shows the prescribed velocity distribution, taken from reference 1. Figure 3(b) presents the velocity distributions obtained from coarse grid, inviscid WIND calculations on both the suction and pressure surfaces at the plane wall. Recall that the elbow shape itself was designed by using inviscid flow analysis. The velocity distributions on both surfaces of figure 3(b) are smooth representations of the prescribed distribution. The differences in shape are attributed to the use of the two different abscissae. Arc length s and index i both depict passage along the channel. However, the use of index i, with recourse to figure 2(b), provides a greater perception of location within the elbow. Finally, figure 3(b) reveals that the calculated exit velocity is about twice the inlet value, in accordance with the inverse ratio of their flow areas. The offset of the two curves in figure 3(b) is caused by the lateral displacement of the suction and pressure surfaces.

Comparison of theoretical velocities in flow field with those computed by wind.—Figure 4(a), taken from reference 1, presents contours of constant theoretical velocity and constant flow angle throughout the channel obtained by the two-dimensional design of reference 1. For comparison, WIND was run using the coarse grid, inviscid input file. Constant Mach number contours from these calculations appear in figure 4(b). This figure was plotted at the midspan location (k = 1) to be as representable as possible to the two-dimensional theoretical plot of figure 4(a). No contours of constant flow angle are shown in figure 4(b). However, the flow structures of the theoretical treatment and the current analysis are similar.

Viscous Turbulent Flow Results

The calculations that were made to produce the figures that follow are for compressible viscous turbulent flow using the fine grid described previously. The Spalart Alimaras turbulence model was used in all subsequent calculations, except in the comparison with various other turbulence models that is presented at the end of the discussion of the results.

Convergence history.—An encouraging result yielded by WIND is the convergence history of the norm of the residuals. Figure 5 presents the norm as a function of iteration number. In most of the WIND results presented, 2000 iterations were used. However, figure 5 reveals that after an initial spike at about 50 iterations, convergence was essentially achieved before 600 iterations.

Onset and buildup of passage vortex.—In the following discussion, the readers are asked to assume a position within the channel always looking in the direction of flow as they move towards the exit (i.e., downstream). Figure 2(c) shows the grid at the first cross section (i = 1). Figure 2(d) depicts typical cross sections encountered in these viewpoints. Figure 6 presents a sequence of such views from inlet to exit, showing total pressure contours at selected cross sections normal to the flow direction.

This starting location is the plane for which i = 1 in figure 2(b). At such cross sections, contours at index i (in the flow direction) from 1 to 75 (the exit) are shown in figure 6. Sides denoted by S and P represent the suction and pressure surfaces, respectively. The open ends denote the midspan (k = 1). The closed sides opposite the open ends represent the plane wall (k = 35).

No boundary layer is shown at the inlet (i = 1). In accordance with the Spalart Allmaras turbulent boundary layer model, a thin boundary layer has already developed at i = 10, and it increases towards the exit (i = 75). During this development, the combination of accelerating flow from the decreasing cross section area and the turning of the 90° bend causes a roll-up of the thickening boundary layer into a passage vortex. This effect is first discernible as a vortex at about i = 60 in figure 6(g). A glance at figure 2(b) shows that this location is near the end of the bend. This is evident by counting back from i = 75 at the exit to i = 60 near the bend in figure 2(b). Note also that the passage vortex has settled into a location on the suction surface that is about one-third of the distance from the plane wall to midspan.

Although the passage vortex depicts a loss in total pressure, it sits on a region of even higher pressure loss. Furthermore, figure 6 shows that a pocket of high total pressure loss also occurs in the corner between the plane wall and suction surface. The exit passage vortex of figure 6(i) is analogous to the trailing edge vortex of an airfoil.

View on X-Z plane.—The readers are now asked to return to the channel inlet, and they are always to face upward to the X-Z planes as they encounter changing orientations along the channel of the elbow. This purpose is achieved by setting constant values of Y. Note that the direction Y is shown in figures 2(a) and (b). Thus, the X-Z planes are cross sections normal to the flow at the inlet, but they are parallel to the flow at the exit. Figure 7 presents total pressure contours from this viewpoint. In figure 7 the suction surface is on the right, and the pressure surface is on the left. The plane wall is at the top, and the midspan is the open end at the bottom.

This second set of contours does not reveal any new phenomena of secondary flow, but it is intended to add insight by taking a different viewpoint. As noted previously, a thin boundary layer soon builds up on all surfaces. As the flow accelerates into the bend, a low pressure region appears in the upper right corner of figure 7(e) at Y = 15.9 in. Within the bend, the low pressure region enlarges, moves away from the plane wall, and an even lower pressure occurs where it meets the suction surface. This observation persists beyond the bend to the exit. These views reveal the inception of the vortex and its development into its maximum size at the exit along the suction surface. These views also emphasize the movement of the vortex away from the plane wall to take up a position about one-third of the distance to the midspan. They further show the deep penetration of the vortex into the mainstream towards the pressure surface.

Comparison with experiments of reference 2.—A comparison of the exit vortex of figure 6(i) (at i = 75) with that obtained experimentally by the work of reference 2, (shown here in fig. 8(a)) is discussed in this section. The smaller size of this calculated exit vortex indicates that use of the Spalart Alimaras turbulence model in WIND results in less secondary flow development. This observation implies that the Spalart Alimaras model is conservative. However, the location of the exit vortex in figure 6(i) closely matches that in figure 8(a). Finally, it was observed that at 500 iterations the exit passage vortex computed by WIND was noticeably larger than at 2000 iterations. Figure 8(b) shows this plot.

Comparison with smoke experiments of reference 7.—A further corroboration of the passage vortex of figure 6(i) appears in figure 9(a). This figure, taken from reference 7, shows the exit passage vortex obtained from smoke flow experiments in a small two-dimensional lucite replica of the elbow designed in reference 1. Reference 7 suggests explanations and hypotheses for the onset and roll-up of the passage vortex. These were derived from the observation of cross channel smoke flow at the plane wall in response to the accelerating and turning shape of the elbow. Figure 9(b), also taken from reference 7, shows cross channel flow of smoke flowing towards the suction surface, where it is crowded into a region away from the plane wall. Note that neither the experimental investigation of reference 2 nor the calculated results from WIND showed any evidence of cross channel flow. Hence, it must be a two-dimensional phenomenon.

Spanwise variation of total pressure contours.—Figure 10 presents the spanwise variation of total pressure calculated by WIND. The views in this figure show contours in the X-Y plane. Progression of the profiles in figure 10 goes from figure 10(a) (plane wall) to figure 10(i) (midspan). Throughout the 24-in. entrance section there is very little loss in total pressure. This observation is revealed by the scarcity of contour lines in the lower parts of figure 10. At and near the plane wall (k = 35 to about k = 27) the loss in total pressure becomes significant in and downstream of the bend because the flow both accelerates and turns. This loss occurs all the way across the channel from the suction surface to the pressure surface. From about k = 27 the development of the aforementioned passage vortex is evident on and adjacent to the suction surface. It appears as a thickening of the suction surface boundary layer in these views. At about k = 20, the boundary layer on the suction surface becomes thinner as the flow straightens towards the exit.

Farther towards midspan (at k = 10 and k = 1) the mainstream flow fills the channel except for a thin boundary layer on the suction surface, and an even thinner one on the pressure surface. See also figure 6(i) for the cross section view at the exit at i = 75.

Finally, figure 9 shows no evidence of cross channel flow, as was noted in the previous discussions.

Spanwise total pressure distribution at exit.—The spanwise exit total pressure distribution as a ratio to inlet total pressure is presented in figure 11. Several cross channel indices from j = 1 to j = 30 were used. Note that in this figure midspan is at Z = 0, and the plane wall is at Z = 8.25 in. Also, j = 1 denotes the suction surface; whereas j = 61 (not shown in fig. 11) denotes the pressure surface. Figure 11 shows that the loss in total pressure at the suction surface is about 20 percent. At the extreme right of this figure, it also shows a 20 percent loss at the plane wall all the way across the channel to the pressure surface (from j = 1 to j = 61). Figure 11 clearly shows the effects of the

passage vortex. The bottoms of the valleys in the curves depict the centerline of the passage vortex. Although the greatest depth and width of any of the valleys occur at j = 20 (the dotted curve), this plot clearly shows that the total pressure loss in the passage vortex is much less than it is on and near the suction surface (j = 1). Finally, at j = 30 (well into the mainstream) the horizontal line at the top reveals that the effects of the passage vortex have been dissipated.

Static pressure variation along elbow profile.—Figure 12 presents the variation of static pressure along the elbow profile at both the plane wall and midspan. Both suction and pressure surface results are shown. Figure 12(a) shows the experimental results of reference 2, and uses velocity potential as abscissa. Figure 12(b) shows the calculated results from WIND, and uses index i as abscissa. The ordinate in figure 12(b) is the ratio (p-pexit)/(ptank-pexit). As noted in reference 2, the exit experimental static pressure in figure 12(a) is slightly greater on the suction surface than on the pressure surface at both the plane wall and midspan. This observation is also shown by the WIND results of figure 12(b). Reference 2 also made this observation for its theoretical analysis and attributed it to overturning of the average flow just upstream of the exit.

Spanwise static pressure variation.—Figure 13 compares the spanwise static pressure variation for both suction and pressure surfaces obtained from WIND with those from the experiments of reference 2. Again, the pressures are shown as ratios. These results are shown at several values of velocity potential for reference 2, and for several values of index i for the WIND results. The plane wall is at Z / W = 0 and the midspan, at 0.5. There is a good comparison between figures 13(a) and (b). As observed in reference 2, the variation in static pressure is slight from the plane wall to midspan at all locations in the direction of flow.

Results from other turbulence models.—Several turbulence models implemented in WIND were tried in this CFD investigation. The standard of merit used in assessing the various turbulence models is the exit passage vortex generated by each model, shown in the Z-Y plane, in comparison with the experimental results of reference 2 shown in figure 8(a). These exit passage vortices are the total pressure contour plots for each model that correspond to that in figure 6(i) at i = 75.

The contour plots for all turbulence models for which the WIND code ran are presented in figure 14. All of these plots were obtained after 2000 iterations. When the results shown in figure 14 are compared with that of reference 2, shown herein in figure 8(a), it is evident that the Spalart Allmaras, Baldwin Lomax, and SST (Shear Stress Transport) models were the most successful. See figures 14(a) to (c). A distant follower was the PDT (P.D. Thomas) model, shown in figure 14(d). Even more distant was the laminar model of figure 14(e).

The laminar result can probably be discredited for the following reasons. The Reynolds number for this investigation is of the order of 360,000. However, reference 8 states that in actual pipe flow, a Reynolds number of the order of 2,000 is sufficient for transition to turbulent flow to occur. This reference further states that under carefully controlled conditions to minimize disturbances, a critical Reynolds number as high as 40,000 has been reached experimentally. Hence, use of the laminar turbulence model is regarded as inappropriate for this investigation.

Finally, reference to figure 14(f) reveals that the inviscid model failed to yield a passage vortex. Nevertheless, the WIND code ran to completion, when using this model.

The WIND code quickly aborted when the following turbulence models were tried:

Baldwin Barth, Cebeci, and Chien.

Previously, this author has tried all nine of these turbulence models in applying WIND to an airfoil designated as RAE 2822, and has documented the results in an unpublished memorandum. For that configuration, WIND ran for eight of the nine turbulence models. Again, the Spalart Allmaras model compared well with experiment. However, the degrees of success of the other models differed from the order found above for the elbow comparisons. Once again, the WIND code failed to run when the Cebeci turbulence model was used.

CONCLUSIONS

This report has presented results for a three-dimensional CFD investigation of secondary flow in an accelerating, 90° elbow. This elbow was designed by NACA in the early 1950's and was used to obtain detailed experimental flow data. Important results of the current CFD investigation and comparison with the NACA data are enumerated below.

1. WIND calculations for flow in a 90° elbow revealed formation of a passage vortex whose development, size, and location matched experimental results. Its shape became discernible as a vortex near the exit of the bend. Several viewpoints are used to display these observations.

2. The passage vortex was caused by pressure gradients induced by the acceleration in the channel and the bend in the elbow.

3. The passage vortex settled on the suction surface about one-third of the distance between the plane wall and midspan. It also projected into the mainstream to about one-third of the channel width.

4. Maximum total pressure loss was about 20 percent, which occurred on the plane wall all across the channel.

5. No separation was observed on either channel wall.

6. The Spalart Allmaras, Baldwin Lomax, and SST turbulence models were the most successful of all of the turbulence models implemented on WIND.

APPENDIX A

Symbols

P	pressure surface
P_o	total pressure, psi
p	static pressure, psi
Q	velocity (expressed as ratio of characteristic velocity equal to constant channel velocity downstream at infinity)
S	suction surface
s	distance in X-Y plane measured along direction of flow (expressed as ratio of characteristic length equal to channel width downstream at infinity)
V	velocity magnitude, ft/sec
X,Y,Z	physical Cartesian coordinates, inches
y+	nondimensional distance from channel wall.
ϕ,ψ	velocity potential and stream function, respectively, used as Cartesian coordinates in transformed plane

APPENDIX B

PRELIMINARY FILES

The input data for the coarse and fine grids, described earlier, were each entered into a separate file.

CCCCCCCCCCCCCCCCCCCCCCCCCCCCCCCCCCCCCCCCCCCCCCCCCCCCCCCCCCCCCCCCCCCC

INPUT DATA FILES

Either of the following two files feeds the input into WIND:

CCCCCCCCCCCCCCCCCCCCCCCCCCCCCCCCCCCCCCCCCCCCCCCCCCCCCCCCCCCCCCCCCCCC

INPUT FILE FOR COARSE GRID INVISCID RUN

```
Stanitz Elbow.
Three-Dimensional, Inviscid Flow.
stan.a.dat

freestream total 0.1 15.422 520.0 90.0 0.0

turbulence inviscid

arbitrary inflow
  zone 1
  total
  hold_totals
  uniform 0.1 15.422 520.0 90.0 0.0
endinflow

mass flow rate actual 14.6 zone 1

convergence order 6
test 128

cfl 2.0

cycle 20
iterations per cycle 100

end
```

CCCCCCCCCCCCCCCCCCCCCCCCCCCCCCCCCCCCCCCCCCCCCCCCCCCCCCCCCCCCCCCCCCCC

INPUT FILE FOR FINE GRID VISCOUS RUNS

```
Stanitz Elbow.
Three-Dimensional, Viscous, Turbulent Flow.
stan.b.dat

freestream total 0.1 15.422 520.0 90.0 0.0

turbulence spalart allmaras
```

```
implicit boundary on zone 1

arbitrary inflow
  zone 1
  total
  hold_totals
  uniform 0.1 15.422 520.0 90.0 0.0
endinflow

mass flow rate actual 14.6 zone 1

/sequence 1 1 1

convergence order 6
test 128

cfl 5.0

cycle 20
iterations per cycle 100

end
```

CCCCCCCCCCCCCCCCCCCCCCCCCCCCCCCCCCCCCCCCCCCCCCCCCCCCCCCCCCCCCCCCCCCCCCCCCCCC

GMAN FILE (Command Form)

The following file incorporates the boundary conditions into the grid file.

```
 FILE stan.cgd
 UNITS INCHES
 ZONE 1
   BOUNDARY I1
     ARBITRARY INFLOW
     UPDATE
   BOUNDARY IMAX
     OUTFLOW
     UPDATE
   BOUNDARY J1
     VISCOUS WALL
     UPDATE
   BOUNDARY JMAX
     VISCOUS WALL
     UPDATE
   BOUNDARY K1
     REFLECTION
     UPDATE
   BOUNDARY KMAX
     VISCOUS WALL
     UPDATE
```

CCCCCCCCCCCCCCCCCCCCCCCCCCCCCCCCCCCCCCCCCCCCCCCCCCCCCCCCCCCCCCCCCCCCCCCCCCCC

REFERENCES

1. Stanitz, John D.: “Design Of Two-Dimensional Channels With Prescribed Velocity Distributions Along The Channel Walls. I—Relaxation Solutions.” NACA TN 2593, 1952.
2. Stanitz, John D., Osborne, Walter M., and Mizisin, John: “An Experimental Investigation Of Secondary Flow In An Accelerating, Rectangular Elbow With 90° Of Turning.” NACA TN 3015, Oct. 1953.
3. WIND Home Page: http://www.grc.nasa.gov/www/winddocs/user/files.html
4. WIND Validation Home Page: http://www.grc.nasa.gov/www/wind/valid
5. Towne, Charles E.: “PLOTC USER’S MANUAL: VERSION 2.3.” NASA internal memorandum, April 1994.
6. Walatka, Pamela P., Buning, Pieter G., Pierce, Larry, and Elson, Patricia A.: “PLOT3D USER’S MANUAL.” NASA, March 1990.
7. Herzig, Howard Z. and Hansen, Arthur G.: “Experimental And Analytical Investigation Of Secondary Flow In Ducts.” Institute Of The Aeronautical Sciences, IAS Preprint No. 593, Presented at the 24th Annual Meeting, Jan. 23–26, 1956.
8. Potter, Merle C. and Foss, John F: “Fluid Mechanics.” Great Lakes Press, Inc.

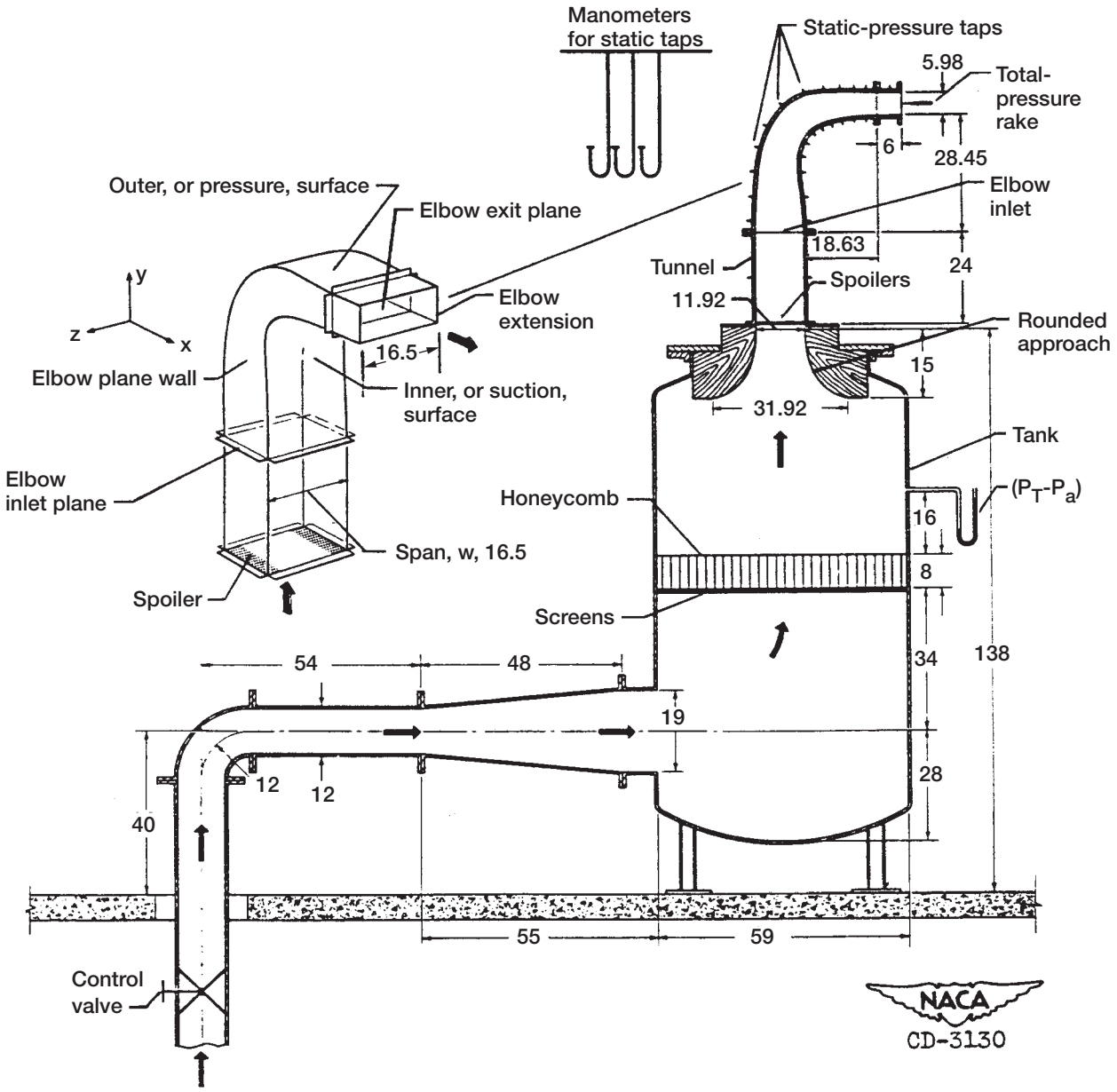

Figure 1.—Line drawing of test setup from ref. 2. All linear dimensions in inches.

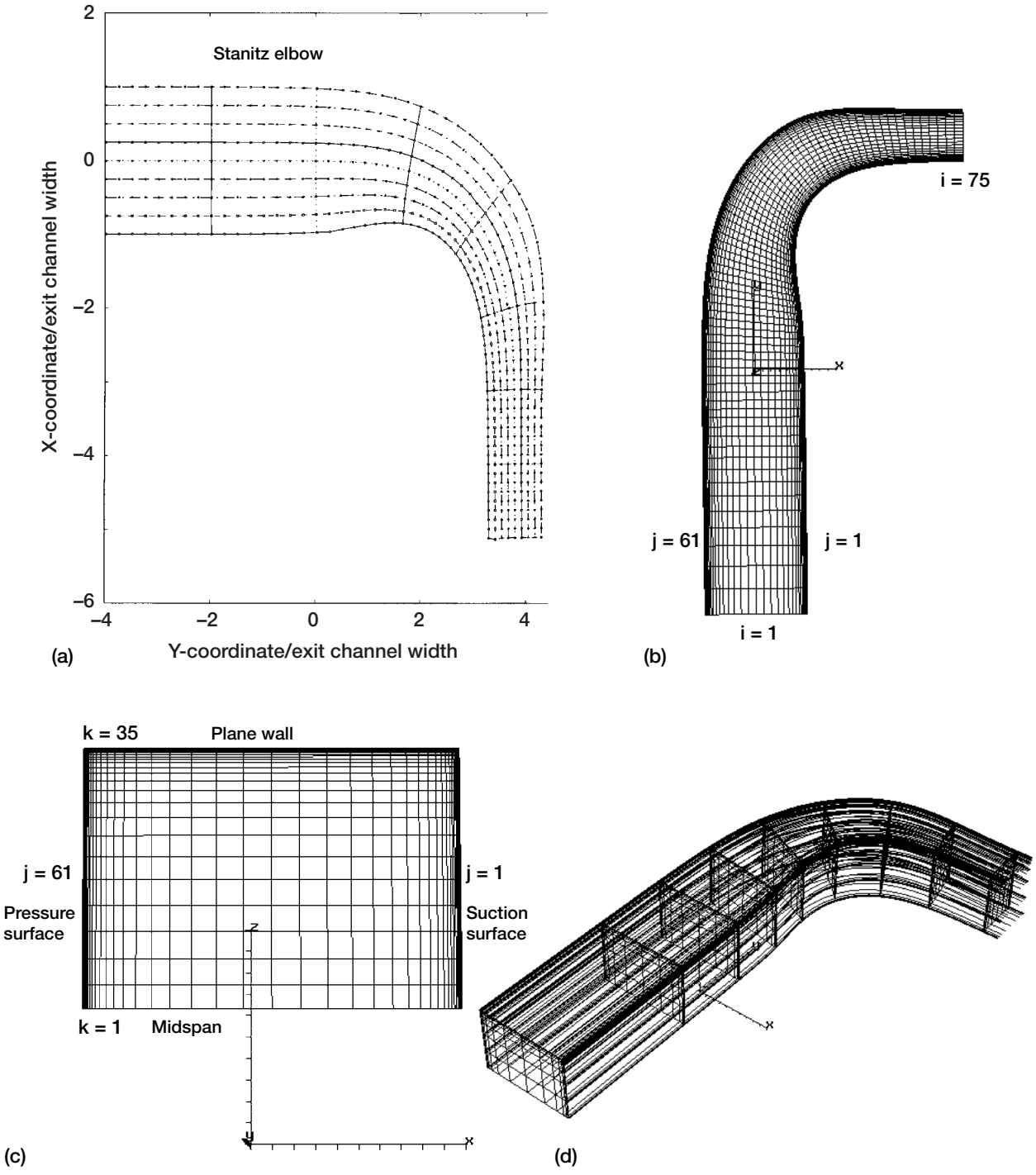

Figure 2.—Grid. (a) Points tabulated in table II of ref. 1. (b) 75x61 in x-y plane at the plane wall (k = 35) (c) 61x35 grid in x-z plane at the inlet (i = 1). (d) 3-D view (thinned) showing planes normal to the flow direction.

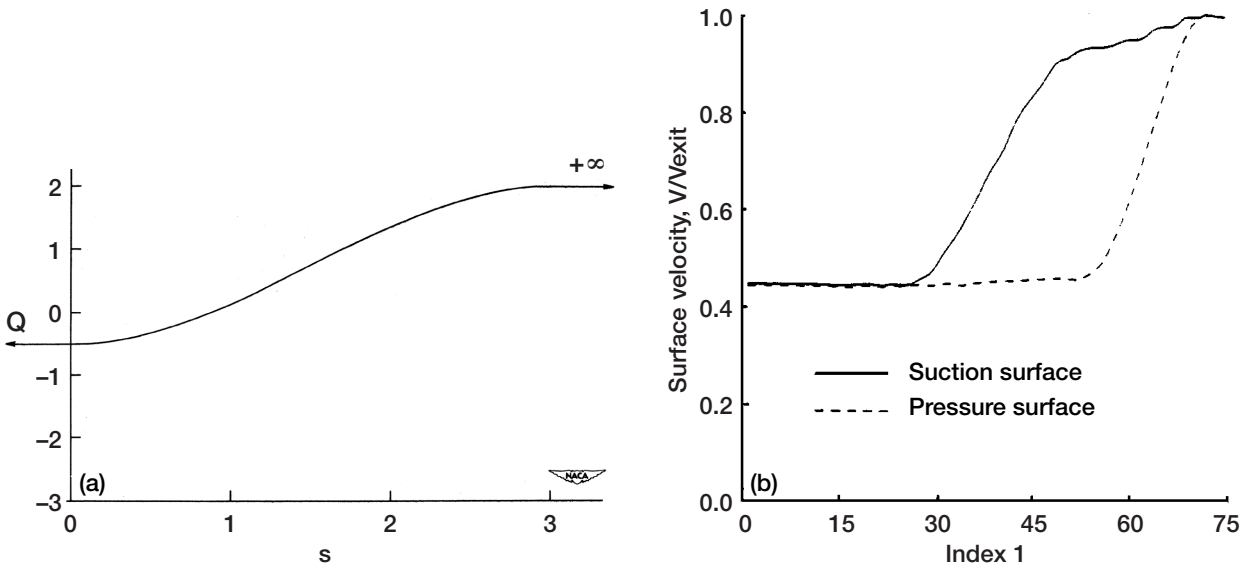

Figure 3.—Surface velocity distribution. (a) Prescribed in ref.1. (b) Wind calculations from coarse grid inviscid run.

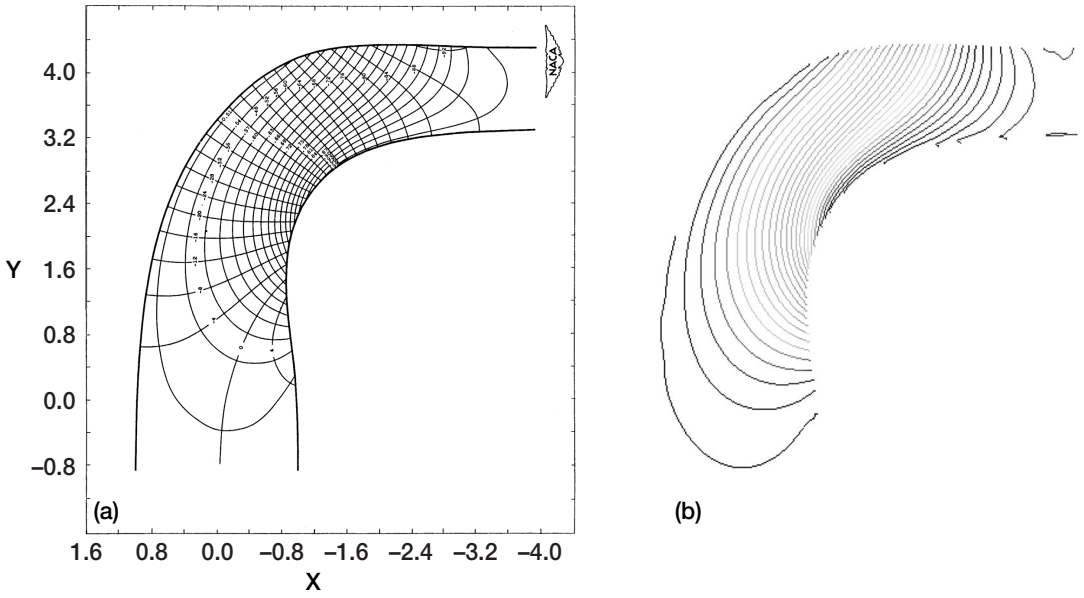

Figure 4.—Velocity contours. (a) From analysis in ref.1. (b) Wind calculations from coarse grid inviscid run.

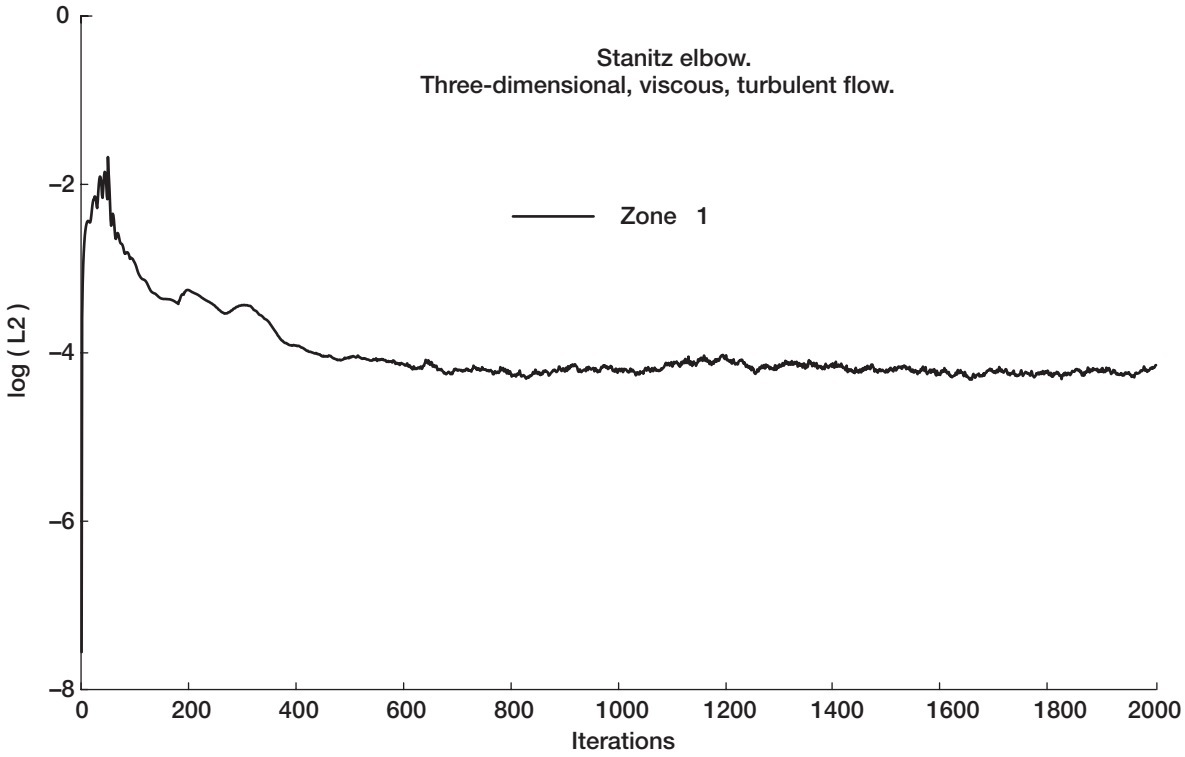

Figure 5.—Convergence history.

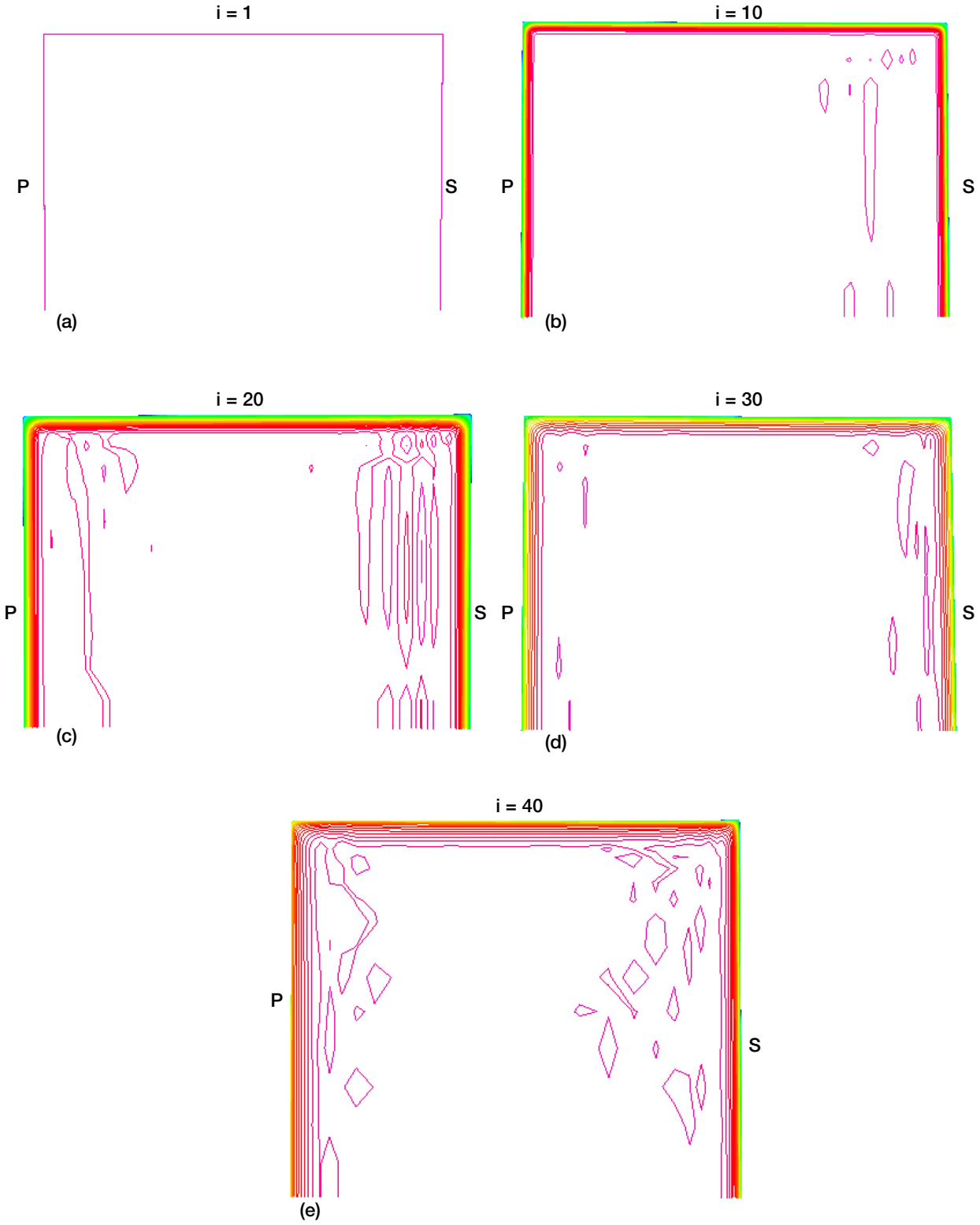

Figure 6.—Total pressure contours at constant i.

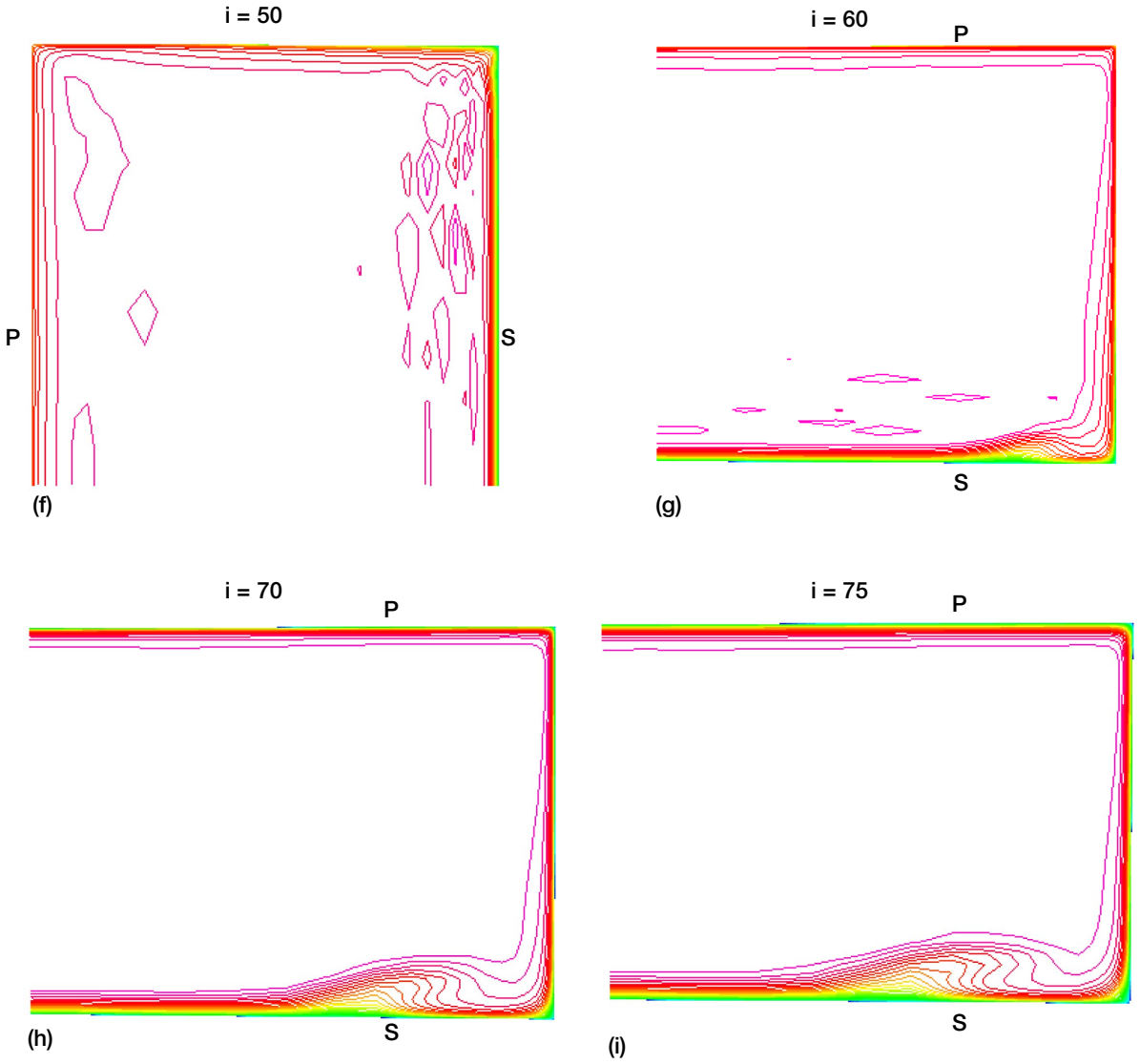

Figure 6.—Concluded.

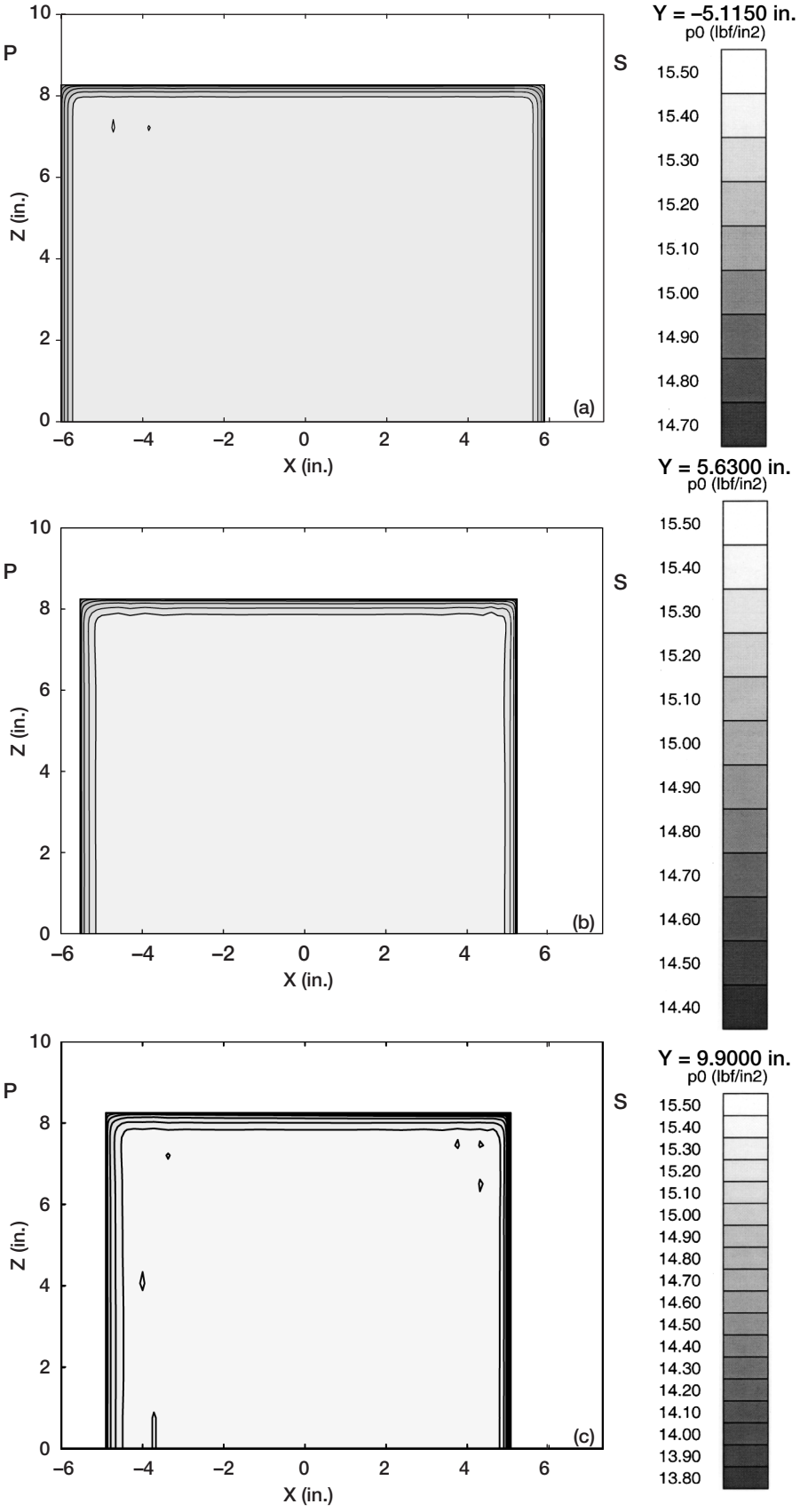

Figure 7.—Total pressure contours in x-z plane.

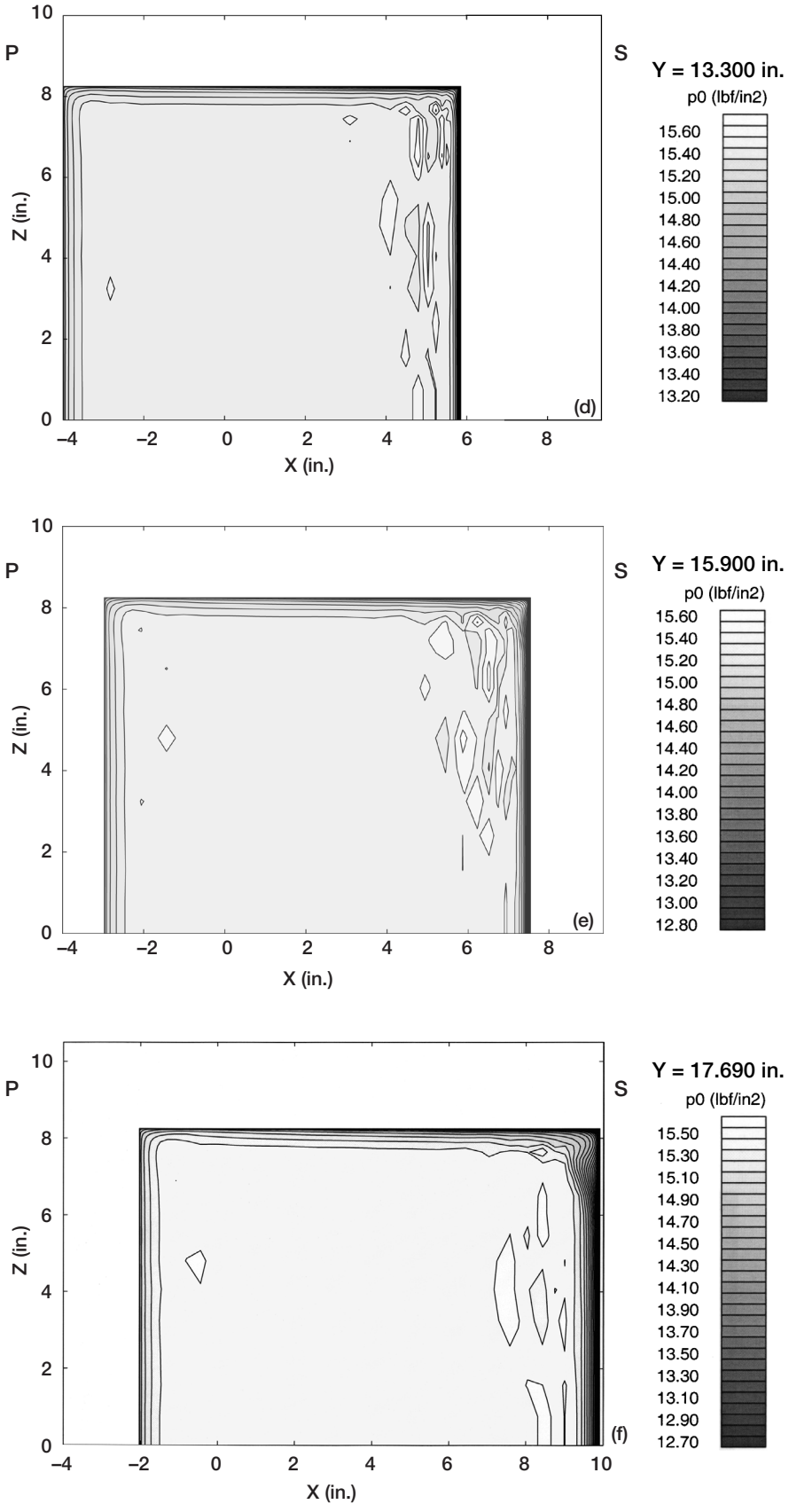

Figure 7.—Continued.

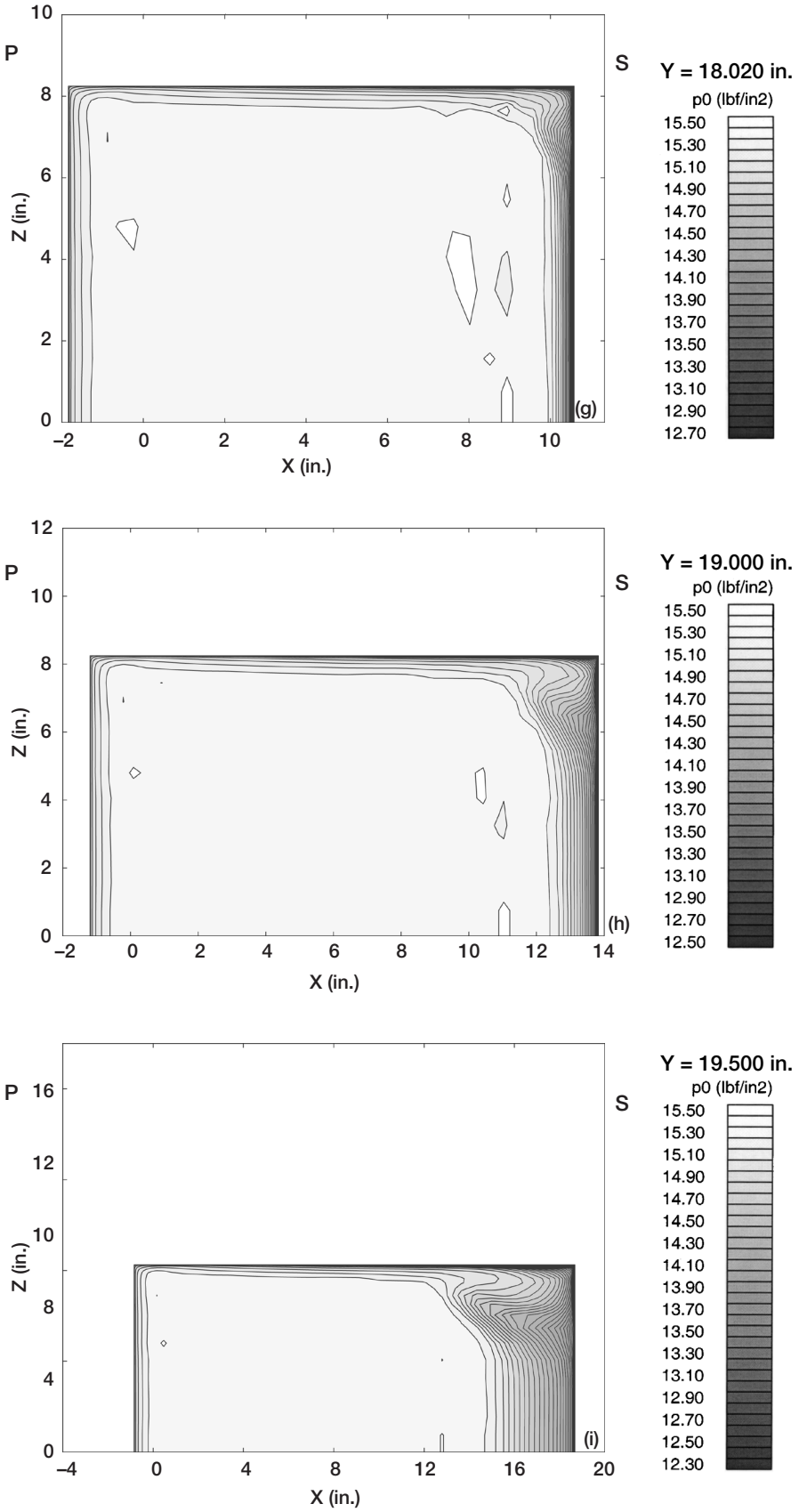

Figure 7.—Continued.

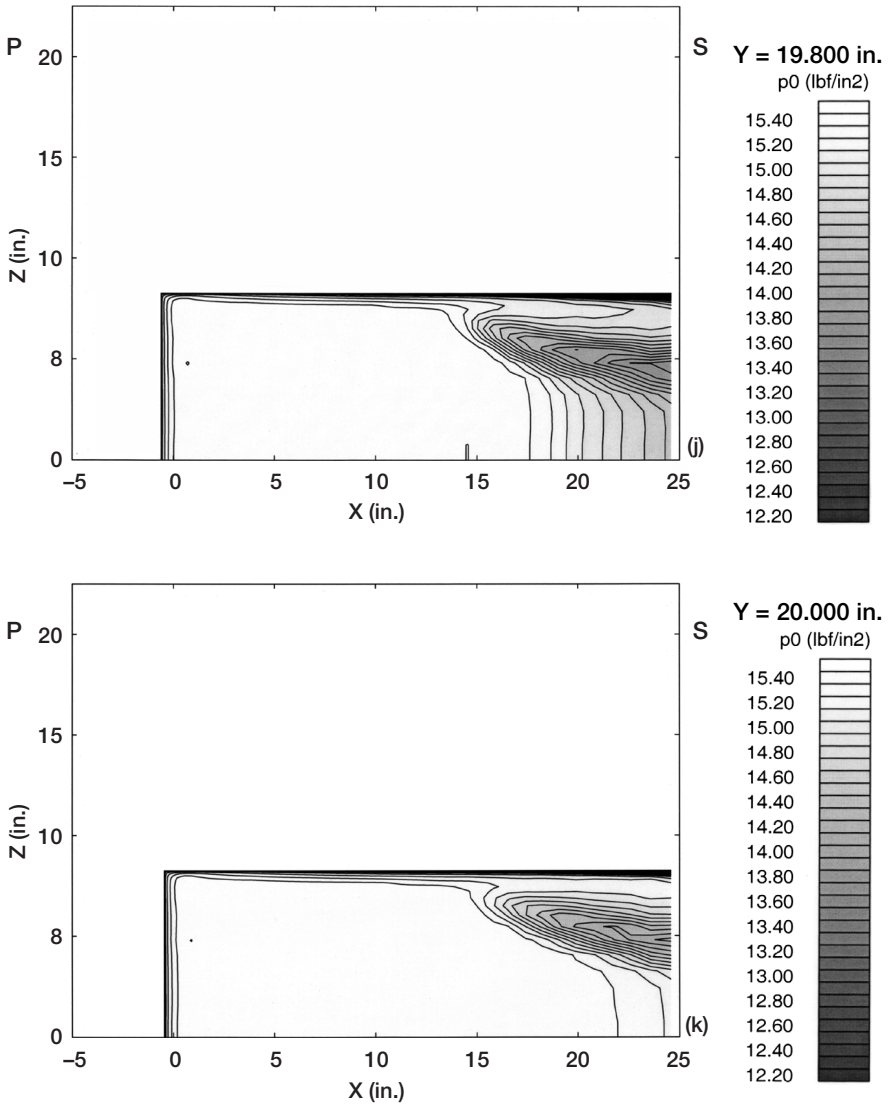

Figure 7.—Concluded.

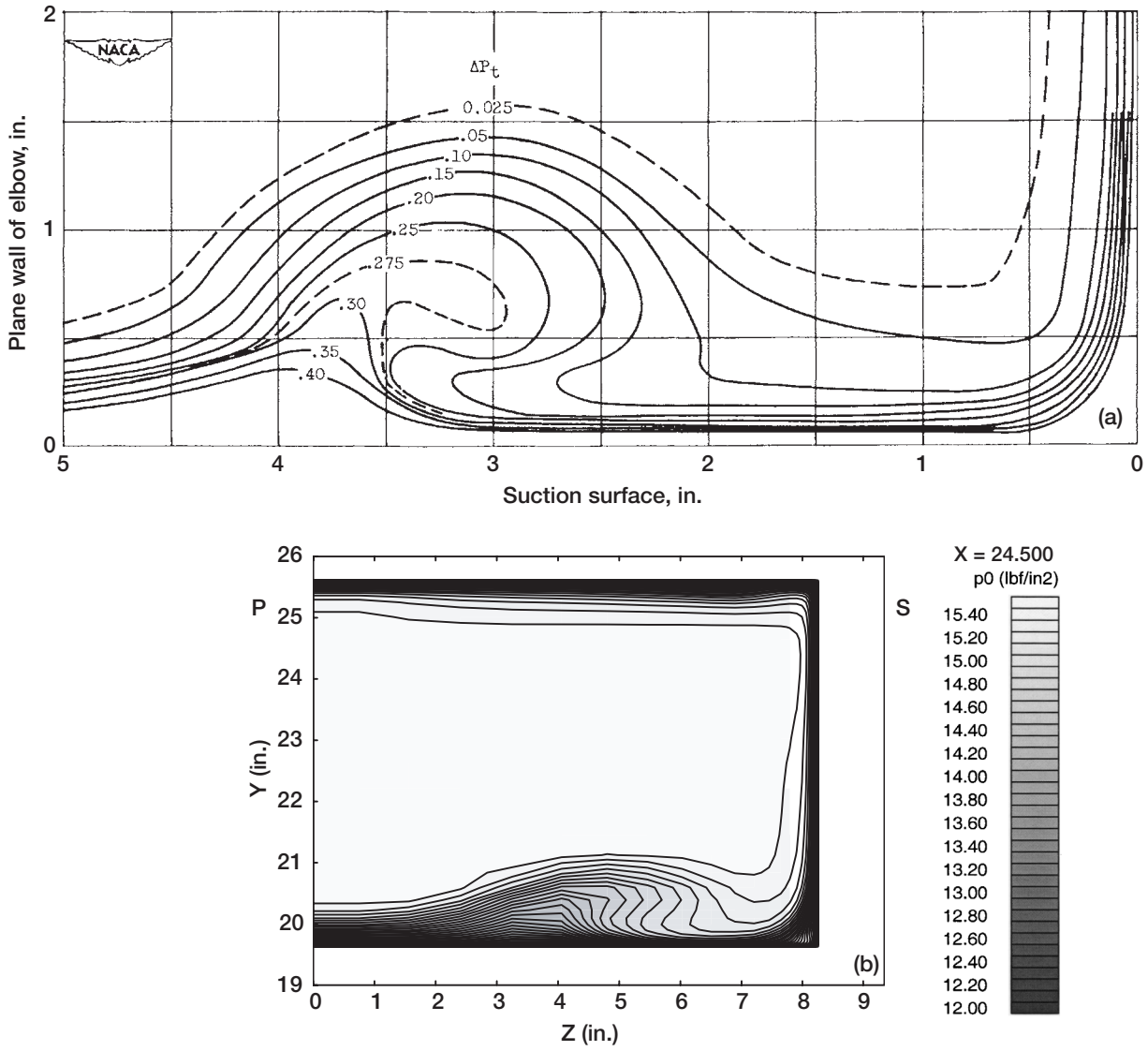

Figure 8.—Total pressure contours at exit. (a) Unshielded total-pressure probe from ref. 2. (b) Wind calculations after 500 iterations.

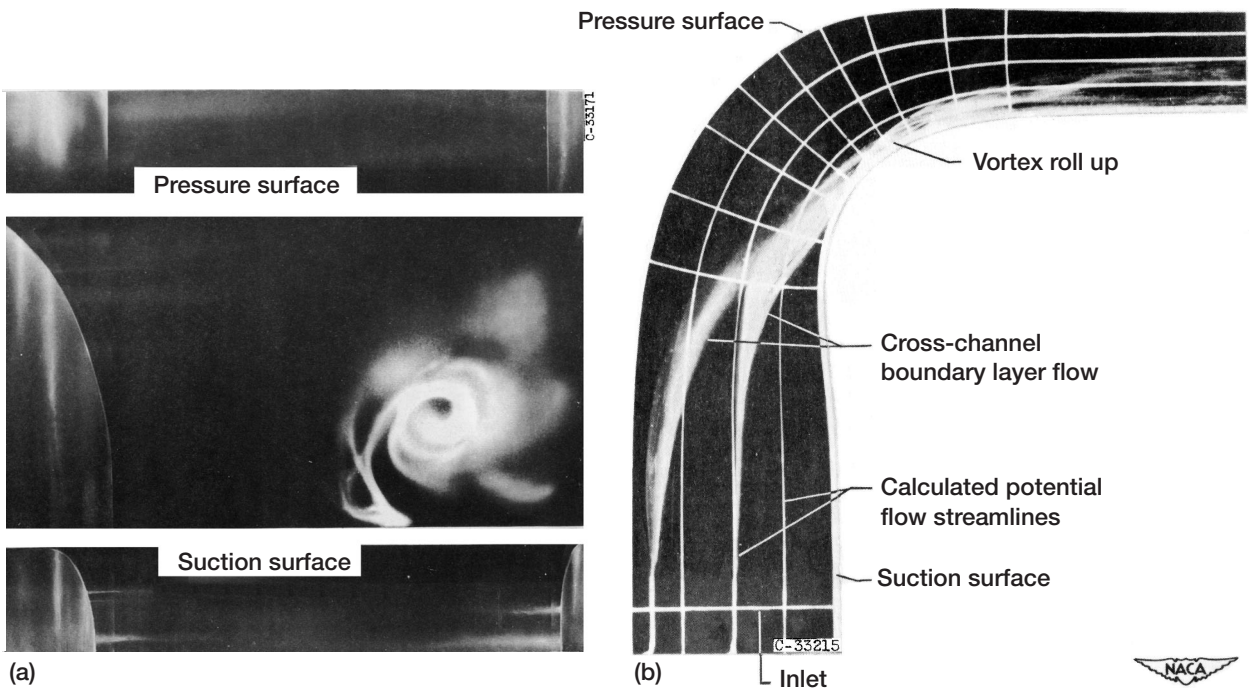

Figure 9.—Smoke experiments from ref. 7. (a) Vortex roll-up at exit of accelerating duct. (b) Cross-channel flow and passage vortex roll-up in 90°-turning accelerating duct.

Figure 10.—Spanwise variation of total pressure contours.

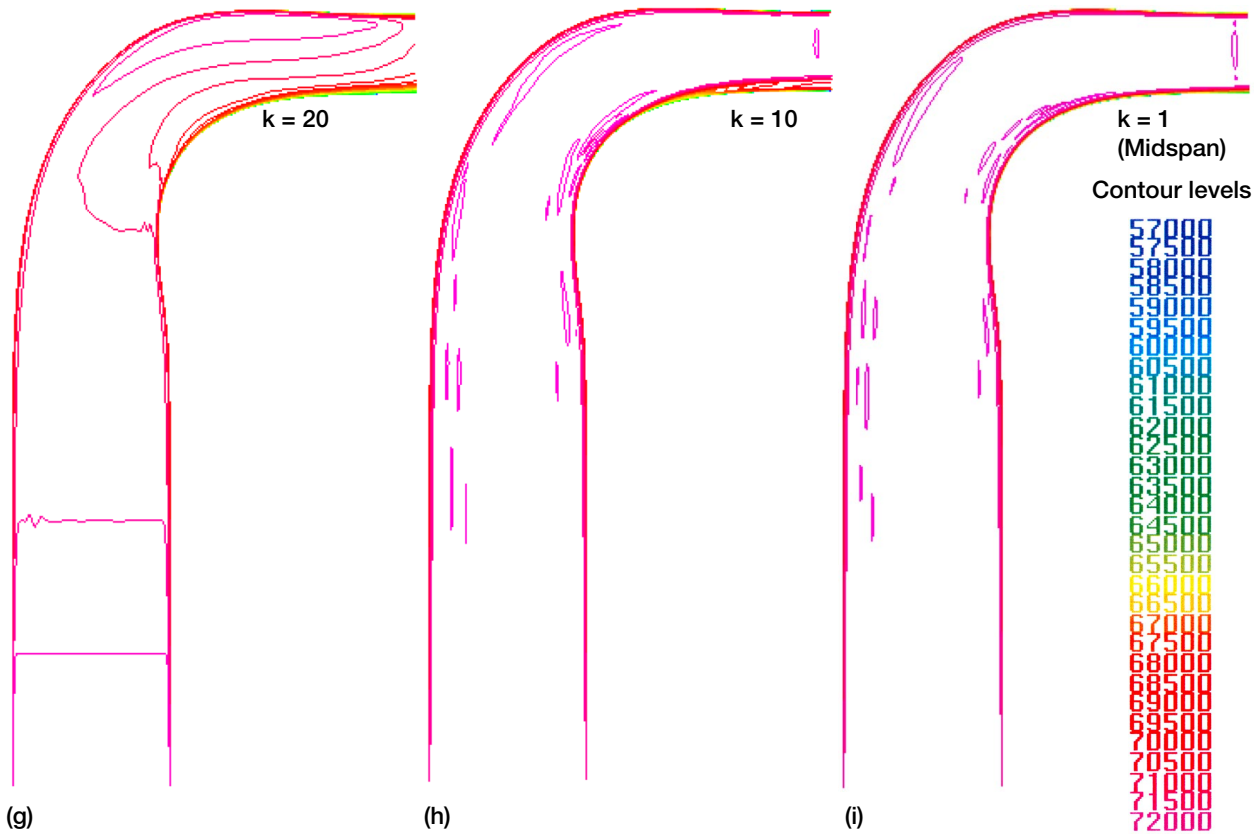

Figure 10.—Concluded.

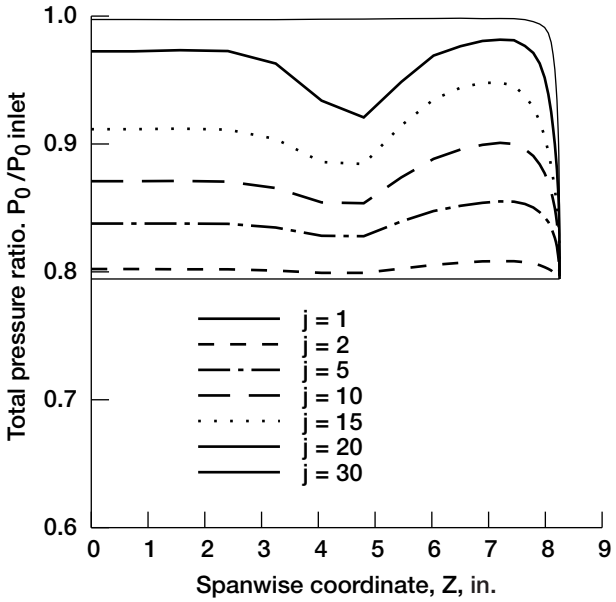

Figure 11.—Spanwise variation of total pressure at exit.

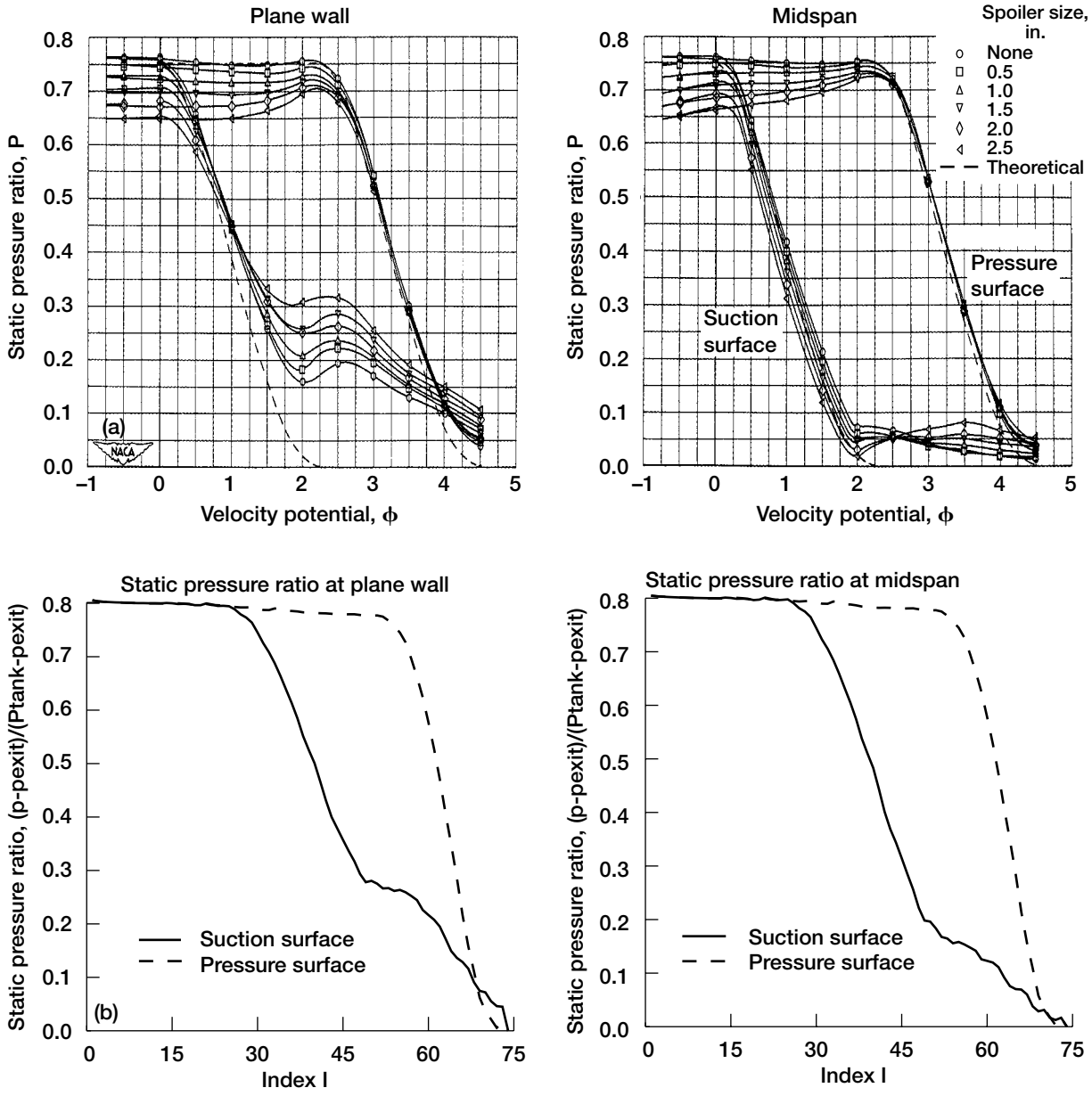

Figure 12.—Static pressure variation along elbow profile. (a) Experimental results from ref. 2. (b) WIND calculated results.

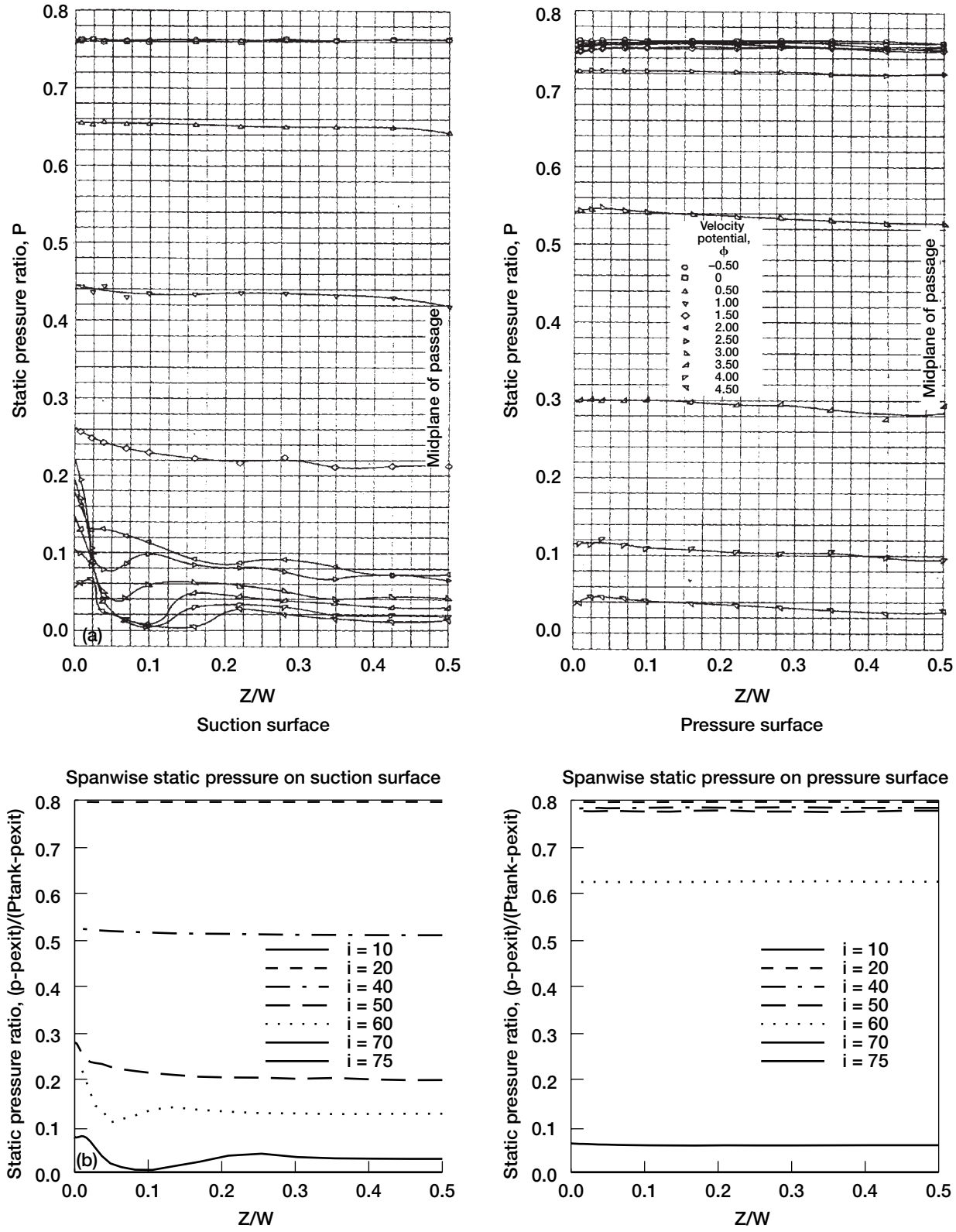

Figure 13.—Spanwise static pressure variation. (a) Experimental results from ref. 2. (b) WIND calculated results.

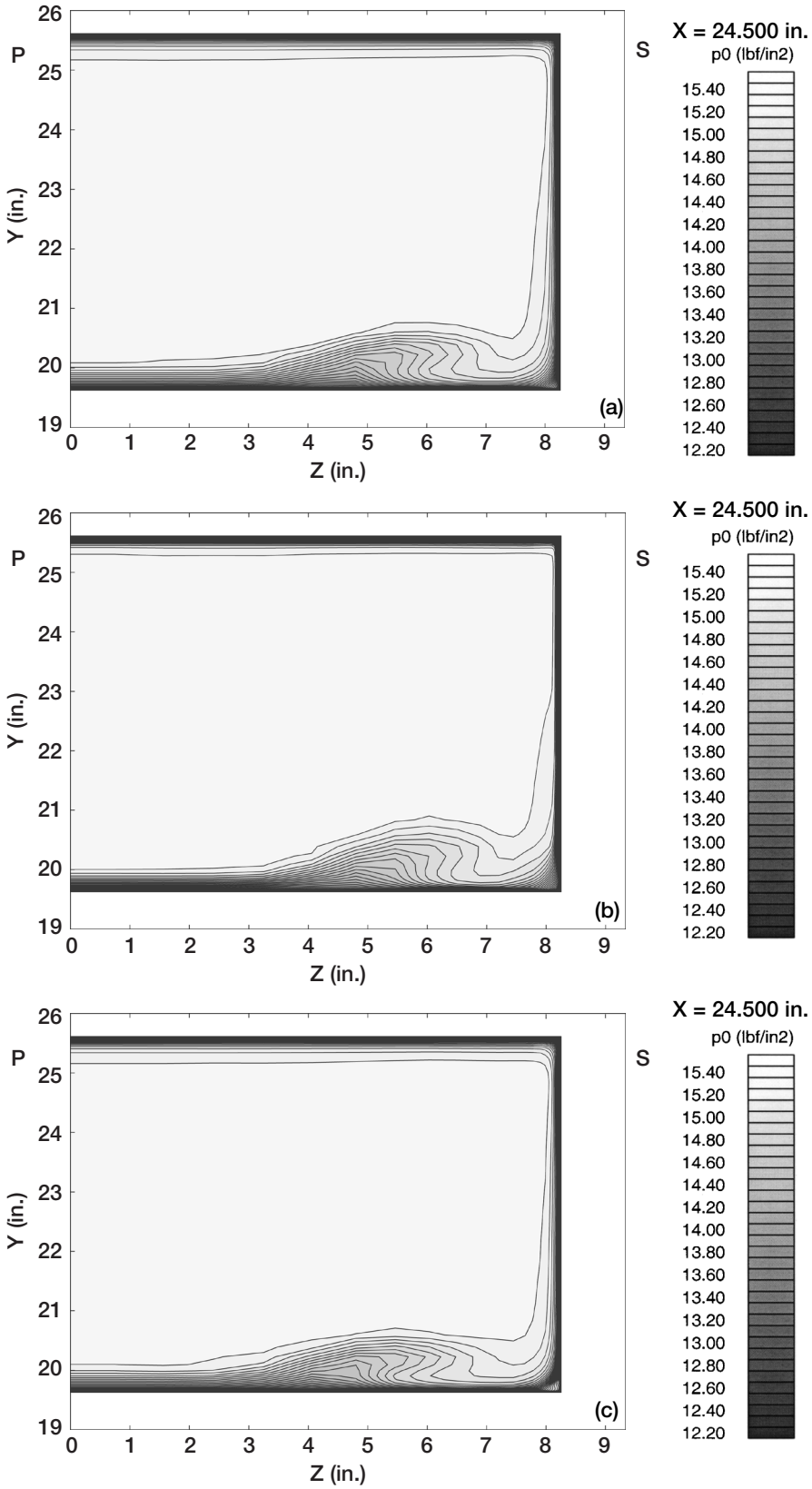

Figure 14.—Rendition of exit passage vortex by several turbulence models. (a) Spalart Alimaras. (b) Baldwin Lomax. (c) SST (Shear Stress Transport) (d) PDT (P.D. Thomas). (e) Laminar. (f) Inviscid.

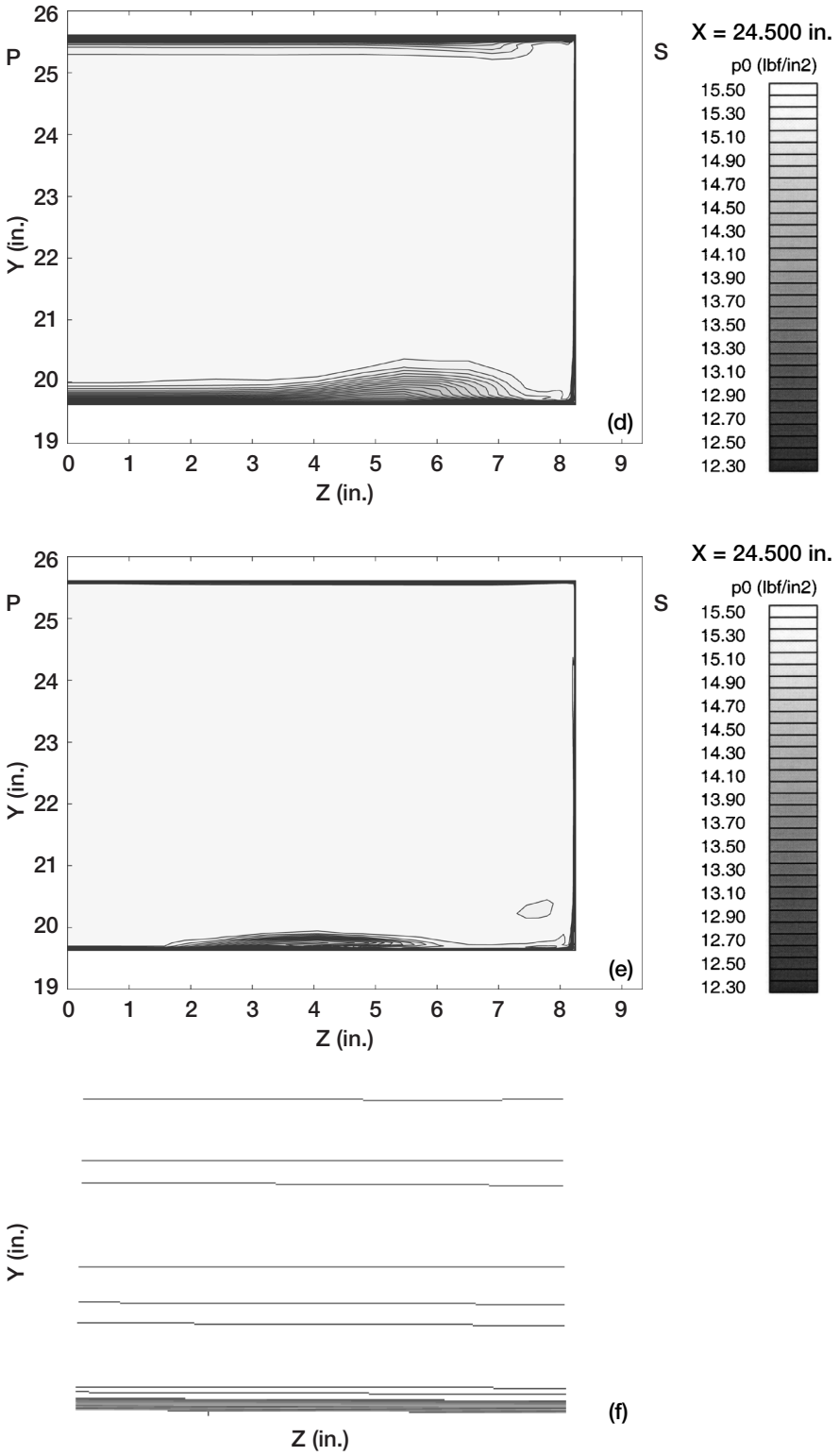

Figure 14.—Concluded. (d) PDT (P.D. Thomas). (e) Laminar. (f) Inviscid.

REPORT DOCUMENTATION PAGE

Form Approved
OMB No. 0704-0188

1. AGENCY USE ONLY (*Leave blank*)	2. REPORT DATE	3. REPORT TYPE AND DATES COVERED
	December 2001	Technical Memorandum

4. TITLE AND SUBTITLE

A Three-Dimensional CFD Investigation of Secondary Flow in an Accelerating, 90° Elbow

5. FUNDING NUMBERS

WU–714–04–50–00

6. AUTHOR(S)

Richard H. Cavicchi

7. PERFORMING ORGANIZATION NAME(S) AND ADDRESS(ES)

National Aeronautics and Space Administration
John H. Glenn Research Center at Lewis Field
Cleveland, Ohio 44135–3191

8. PERFORMING ORGANIZATION REPORT NUMBER

E–13071

9. SPONSORING/MONITORING AGENCY NAME(S) AND ADDRESS(ES)

National Aeronautics and Space Administration
Washington, DC 20546–0001

10. SPONSORING/MONITORING AGENCY REPORT NUMBER

NASA TM—2001-211219

11. SUPPLEMENTARY NOTES

Responsible person, Richard H. Cavicchi, organization code 5850, 216–433–5873.

12a. DISTRIBUTION/AVAILABILITY STATEMENT

Unclassified - Unlimited
Subject Categories: 02 and 34 Distribution: Nonstandard

Available electronically at http://gltrs.grc.nasa.gov/GLTRS

This publication is available from the NASA Center for AeroSpace Information, 301–621–0390.

12b. DISTRIBUTION CODE

13. ABSTRACT ***(Maximum 200 words)***

NASA Glenn Research Center has recently applied the WIND National Code flow solver to an accelerating elbow with a 90° bend to reveal aspects of secondary flow. This elbow was designed by NACA in the early 1950's such that flow separation would be avoided. Experimental testing was also done at that time. The current three-dimensional CFD investigation shows that separation has indeed been avoided. Using its three-dimensional capability, this investigation provides various viewpoints in several planes that display the inception, development, and final location of a passage vortex. Its shape first becomes discernible as a vortex near the exit of the bend. This rendition of the exit passage vortex compares well with that found in the experiments. The viewpoints show that the passage vortex settles on the suction surface at the exit about one-third of the distance between the plane wall and midspan. Furthermore, it projects into the mainstream to about one-third of the channel width. Of several turbulence models used in this investigation, the Spalart Alimaras, Baldwin Lomax, and SST (Shear Stress Transport) models were by far the most successful in matching the experiments.

14. SUBJECT TERMS	15. NUMBER OF PAGES
Secondary flow	35
	16. PRICE CODE

17. SECURITY CLASSIFICATION OF REPORT	18. SECURITY CLASSIFICATION OF THIS PAGE	19. SECURITY CLASSIFICATION OF ABSTRACT	20. LIMITATION OF ABSTRACT
Unclassified	Unclassified	Unclassified	